Master's Thesis

MODELLING THE COMETARY PLASMA ENVIRONMENT IN PREPARATION FOR COMET INTERCEPTOR

Swedish Institute of Space Physics (IRF) - Uppsala, Sweden

Lilou BERNARD

2023/2024

Supervisors: Niklas EDBERG, Pierre HENRI, Anders ERIKSSON, Erik VIGREN

Dates: from March 14th to August 23th 2024

PREFACE

During the last year of my studies, I was enrolled in two masters degrees: Space Engineering, and Planetary Sciences & Space Exploration, and when it came to choose a master's thesis project, I naturelly decided to try to find a research project which will allow me to be implied in a space mission, and then keep my doors open whenever to apply for a Ph.D., or for a job. Moreover, I was decided to look for an opportunity in Sweden, as it was a dream for me to live there, and that was the perfect experience to do it so.

I finally find a project that suits me perfectly well at the the Swedish Institute of Space Physics in Uppsala, Sweden (*Appendix 1: Presentation of the institute*).
Indeed, in addition to have all the requirements I wanted for my master's thesis, this project's goal concerns comets and plasma physics, which were my favorites courses this year.

The purpose of this master's thesis is to model the cometary plasma environment, in preparation to the ESA Comet Interceptor space mission. More specifically during the first part of the project, we were trying to understand how the bow shock of the comets evolves with the heliocentric distances and outgassing rates. A second part of this research project, we will complete the study of the cometary plasma environment by doing again the same work but with two other boundaries: the diamagnetic cavity and the exobase.

Pour ma dernière année d'études, j'étais inscrite en double diplôme: Ingénierie Spatiale, et Sciences Planétaires et Exploration Spatiale. Quand il a fallu choisir un sujet pour mon stage de fin d'étude, il était évident pour moi de chercher un projet de recherche qui me permettrait d'être impliquée dans une mission spatiale, notamment pour me laisser la possibilité de postuler à un doctorat ou à un emploi à la fin de celui-ci. De plus, j'ai décidé concentrer mes recherches de stage de fin d'étude en Suède, car je rêvais d'y vivre depuis plusieurs année, et c'était donc pour moi enfin l'occasion de réaliser ce projet qui me tenais à coeur.

J'ai finalement à trouver ce projet à l'Institut suédois de physique spatiale à Uppsala, en Suède (*Annexe 1: Présentation de l'institut*). En effet, en plus de répondre à toutes les exigences que je souhaitais pour mon stage de fin d'étude, l'objectif de ce projet concerne les comètes et la physique des plasmas, qui étaient mes cours préférés de cette année.

Le but de cette thèse de master est de modéliser l'environnement plasma des comètes, en préparation de la mission spatiale Comet Interceptor de l'ESA. Pour cela, nous avons essayé dans la première partie de ce projet de comprendre comment le choc se formant au devant des comètes évolue en fonction de leurs distances héliocentriques et leurs taux de dégazage. Dans une seconde partie du projet, nous compléterons cette étude de l'environnement plasma des comètes en refaisant le même travail mais sur deux autre frontières : la cavité diamagnétique et l'exobase.

ABSTRACT

The objective of this research was to model the cometary plasma environment in order to prepare for the Comet Interceptor mission. In other words, the main goal was to determine the outermost plasma boundary to be encountered by Comet Interceptor, i.e. the bow shock, to know the scale size of potential comet targets. The bow shock is the boundary formed where the solar wind first meets the comet. We determine the bow shock stand-off distance potential Comet Interceptor mission targets, if the spacecraft had already been launched. These comets were specifically selected by the project team because they were reachable within the mission's operational lifetime, if it had been already launched.

The study investigated the relationships between tree boundary distances (bow shock, diamagnetic cavity and exobase), heliocentric distance, and outgassing rates of the comets. Furthermore, the Rosetta spacecraft's trajectory has been studied in relation to the bow shock location of its target 67P/Churyumov-Gerasimenko, in order to determine potential interactions with the comet's bow shock boundary. We also modelled theses locations for comet Hale Bopp to get an upper limit to the scale size of potential targets.
The stand-off distance of each comet's bow shock was determined using the model developed by Koenders et al. (2013) after having first scaled the model parameters (outgassing rate, ionisation rate, Solar wind parameters) by heliocentric distance. For the diamagnetic cavity, the Cravens et al. (1986) model was used while the Henri et al. (2016) model was applied in order to calculate the exobase location.
For comet 67P and the selected dataset, our results clearly show that the bow shock stand-off distance relies on the heliocentric distance. Beyond about 2 AU, the bow shock did not form at all for 67P. For Hale-Bopp, the bock shock was much larger and reached a few times 10^6 km at a heliocentric distance at 4 AU. Furthermore, we could also study how the stand-off distance increased with the comet's outgassing rate. Regarding the diamagnetic cavity, they have approximatively the same size (around 10^3 km at 1 AU) than the exobase for the selected dataset of comets, while 67P sees a difference with a factor 10 between the size of the diamagnetic cavity (≃100 km at perihelion) and the exobase (≃10 km at perihelion).

These results are crucial for understanding dynamic interactions between comets and the solar wind, particularly as comet 67P approaches within 1.6 AU of the Sun, a phase when the bow shock can extend sufficiently to intersect with spacecraft trajectories like Rosetta's.

TABLE OF CONTENTS

INTRODUCTION

In the vastness of the universe, a lot of celestial phenomena captured human interest and imagination since thousand of years, and among them, comets hold a special position. For as long as anyone can remember, these travelers have been visible in the night sky, enchanting people with their breathtaking beauty. Just like shooting stars, they sparkle through the dark, leaving behind a trail of wonder and amazement.

This project focuses on modeling the cometary plasma environment, in preparation for the Comet Interceptor mission; in other words, the goal of this project is to study the evolution of three bouderies (the bow shock, the diamagnetic cavity and the exobase) based on cometary parameters such as the distance from the Sun (heliocentric distance) and the outgassing rates, in order to prepare the study of the comet which will be observed by Comet Interceptor. The bow shock is the outer most plasma boundary that forms when the solar wind interacts with the comet, and is the first boundary that Comet Interceptor will encounter. The diamagnetic cavity corresponds to the region where the solar wind magnetic field is significantly reduced or even absent, and the exobase defines a limit between a region where the collision between the gas particules are significant and a region where they are so sparse that they can escape into space without colliding with other particles.
In order to reach the goal of this project, we used different models; for the bow shock one, it also has been refine through the addition of complexifications; the methods we employed will be presented, just like the results and their interpretation. We have opted to present the results chronologically for clarity and coherence, respecting the sequence of the work.

1. Comets

For many years, comets have been the focus of extensive research. As a result of our ongoing research, comets are now understood to be more than just astronomical displays; they are cosmic archives that hold the secrets of the past (Brooke, 1998). Some of the elements necessary for life itself are contained within the frozen embrace of cometary nucleus; in fact, their main constituents are dust, water ice, carbon dioxide (CO_2) ice, carbon monoxide (CO) ice, and methane (CH_4) ice (Götz et al. 2022). It has been suggested that comets were essential in providing our planet with water and facilitating the emergence of life on Earth due to their makeup (Hartogh et al. 2011).

Comets formed in the beginning of our solar system; currently, they are primarily imprisoned in the Oort Cloud (20 000-100 000 astronomical units (AU), Vokrouhlicky et al. 2019) and the Kuiper Belt (30-55 AU, Jewitt et al. 2019). Comets are important witnesses to the history of our solar system because these cold, far-off areas of the solar system have maintained their chemical and elemental composition intact for billions of years.

Comets are believed to have formed in the cold primordial disk. They claimed to be leftovers from the formation of the solar system 4.5 billion years ago, and are among the oldest and most primitive objects we know in terms of chemical composition (Davidsson et al. 2015). Their research offers important new perspectives on the circumstances and mechanisms that governed the solar system's creation. There are comets from beyond our solar system, known as instellar comets, that are located in the expanse of space. At that

time, only two interstellar comets already have been observed : 1I/Oumuamua and 2I/Borisov (Bailer-Jones et al., 2020); they inspire us to explore and learn more about the secrets of the cosmos by providing us with fascinating insights into far-off regions of our cosmic home.

However, in the goal to learn more about comets, missions are becoming more ambitious and technically advanced. For instance, in 2005, the Deep Impact mission deliberately collided with Comet 9P/Tempel, in 2016, the Rosetta mission orbited Comet 67P, and in 2015, the Philae lander settled on the same comet.

To come back to the characteristics of the comets, they follow an elliptical orbit around the Sun and, due to their composition, do have highly variable activity. As they approach the Sun, their surface heats up, causing the ice present on and near their surface to sublimate, from about 3 AU. The outgassing rate, which measures the amount of water vapor emitted by a comet per unit time, can be derived from measurements by using instruments located on Earth (ground-based, remote) or in space (remote, in situ).

The Haser model allows for predicting the neutral density of species assuming a spherically-symmetric homogeneous outgassing of species, using an exponential term with a constant radial velocity (Götz et al, 2022). The sublimating material (gas emitted) is not gravitationally bound, and expands freely around the comet nucleus. The density of the neutral gas around the comet is

$$n_s(r) = \frac{Q_0, s}{4\pi U_{n,s} r^2} * e^{-(r-r_c)*\frac{k_{p,s}}{U_n, s}} \quad \simeq \quad \frac{Q_0, s}{4\pi U_{n,s} r^2} \qquad \text{(Eq. 1)}$$

where $Q_{0,s}$ the total outgassing rate of species in s^{-1}, $U_{n,s}$ its velocity (also refered to as the neutral velocity) in $m.s^{-1}$, r the nucleus radius in m, r_c the cometocentric distance in m, $k_{p,s}$ the total photo-destruction rate of the species in s^{-1}, and n_s the neutral density in m^{-3}.

This outgassing phenomenon creates an envelope around the cometary nucleus. The outgassed material forms an atmosphere that is not bound by gravity, expanding radially outward. As it interacts with the solar wind, this material becomes ionized, creating an ionosphere and magnetosphere around the comet, and promoting the development of a plasma environment around the nucleus.

According to Götz et al. (2022), three states of outgassing rates along the 67P comet's trajectory can be identified to classify and obtain spatial scale information (*Appendix 2 : Illustration explaining the three stages of 67/P outgassing rate*).

- Strongly active stage for $Q > 5\times10^{27}\ s^{-1}$
- Intermediately active stage for $10^{26} < Q < 5\times10^{27}\ s^{-1}$
- Weakly active stage for $Q < 10^{26}\ s^{-1}$

The solar wind is a supersonic stream of charged particles that are expelled from the Sun's corona, mostly protons and electrons. Owing to the elevated coronal temperatures, this wind expands into space and generates the heliosphere, a bubble that stretches well beyond Pluto's orbit, and travels at velocities between typically 300 and 800 km/s. The solar wind has a big impact on comet appearance. As a comet approaches the Sun, the solar wind sweeps ions from it, creating an ion tail that is always facing away from the Sun. Comets' distinctive appearance during solar system transit is caused by this interaction between the solar wind and cometary ions. When the solar wind encounters the comet plasma, it causes a

deceleration known as the bow shock and illustrated on the Figure 1 below, from Götz et al (2022).

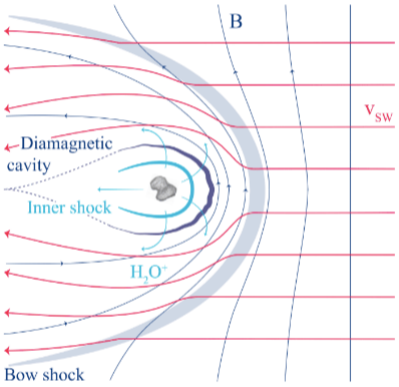

Figure 1: Schematic representation of the different layers in an intense plasma environment (Götz et al. 2022)

A comet is seen in Figure 1 with the nucleus at the center, and the solar wind is moving from right to left. The comet shows strong plasma activity, and several envelopes can be seen forming as a result of the outgassing. The bow shock, which is produced by the interaction of the solar wind and the comet, is represented by the first grey shaded band visible from the right. In addition, we can see two other boundaries; the dark blue boundary borders a region known as the diamagnetic cavity, and originates from the interaction between the comet's outgassed material and the Solar Wind, and the light blue one represents the inner shock boundary, under which the expansion velocity exceeds the speed of sound.

2. The Comet Interceptor space mission

Comet Interceptor is an European Space Agency (ESA) mission scheduled to launch in 2029. It is a very interesting and unique space mission as it will be the first mission to visit a comet coming directly from the outer solar system, developed in collaboration with JAXA, and allowing the study of a pristine and long period comet as unchanged as possible since the dawn of the solar system (Jones et al., 2024). This mission consists of three different probes and various instruments involving several countries, including France and Sweden. The main goal of the mission is to closely study a pristine, long-period comet or interstellar object to among several things, study the 3D structure of the plasma environment, and determine the similarity to short-period comets and their potential role in the emergence of life on Earth.

The concept behind the Comet Interceptor mission is unique, as unlike previous space missions, no specific target comet has been predefined. The spacecraft will after launch, patiently await the passage of an interesting comet.
After launch, the spacecraft will transfer to, and park at the Sun-Earth L2 Lagrange point, wait until a suitable, untouched comet appears. Upon identifying such a target, the spacecraft will maneuver to flyby the comet, deploying two probes to observe it simultaneously from multiple angles (Jones et al., 2024).

The Swedish Institute of Space Physics (IRF) is heavily involved in the mission, especially in the development of two instruments: the Cometary Plasma Light Instrument (COMPLIMENT) and the Solar wind Cometary Ions and Energetic Neutral Atoms (SCIENA).

COMPLIMENT is being developed as collaboration between IRF Uppsala, BIRA in Belgium and under the lead of LPC2E/Orléans and Nice Observatory. SCIENA is being developed at IRF Kiruna.

The preparatory stage is crucial because the comet that the mission will be targeting has not yet been identified. As a result, in order to enable an early assessment of the comet's characteristics, the sensors must be prepared to measure in the right range, with the right settings and the right time. Comets that are within a range of distances and features that permit a feasible contact with the spacecraft are considered interceptable comets, such that Comet Interceptor can study and reach them. Important characteristics for target selection include the comet's magnitude, inclination, orbital period, and distance from Earth. These parameters affect the likelihood of success and the scientific value of the gathered data, and are considered when deciding which comet is most suited for Comet Interceptor in the end.

3. The Rosetta space mission

As we in this study are interested in the evolution of the bow shock, and its evolution with heliocentric distance, we will also apply a comet's bow shock model to the actual data gathered by the Rosetta mission.

Launched in March 2004, the Rosetta space mission tracked Comet 67P/Churyumov-Gerasimenko along its orbit around the Sun and placed the Philae lander on its surface in order to investigate the comet (Glassmeier et al., 2007). Because so much data was collected throughout the trip, this particular comet stands out as one of the most researched celestial bodies; 67P is well-known for having a large data set that provides extensive knowledge on planetary formation and comet science. Rosetta's instruments made possible the precise observations and have substantially advanced our understanding of cometary behavior and the bigger processes occurring in the solar system.

4. Selection of the data for the project

To model the cometary plasma environment, we primarily utilized data from « Horizon » (https://ssd.jpl.nasa.gov/horizons/), the ephemeris system of the NASA Jet Propulsion Laboratory (JPL). This system stores information on celestial bodies and offers unlimited open access to these data for researchers, astronomers, and the general public. Among other things, Horizon can be used to schedule space missions or plan for observations. Along with other data throughout time, it offers details on the motion, observability, and trajectories of various Solar system bodies. A previous investigation by the Comet Interceptor project team used data from « Horizon » to create a list for Comet Interceptor targets, generated on November 3, 2023. To accomplish this, several filters were applied to select comets:

1. The first selection was based on the cometary orbital parameters; data were chosen for comets with perihelion distance ($q_{perihelion}$) less than 1.5 astronomical units (AU) as the mission cannot go farter from the Sun, aphelion distance ($q_{aphelion}$) greater than 100 AU, and data arc longer than 30 days. The first selection also includs those with Q = INDEF.

2. Among this first selection, comets with a total number of observations (N_{obs}) less than 30 or an orbit fit quality code greater than 5 were rejected due to data quality and precision concerns.

3. Finally, the heliocentric distance at two node crossings (ascending and descending, the two notes where the comet orbit intersects the ecliptic plane) was calculated, and only comets with heliocentric distances between 0.7 and 1.5 AU were retained.

We directly used the selected dataset to find the data we needed, which are the outgassing rates (Q) calculated from remote observations, and the heliocentric distances (R_h) at which the outgassing rates were measured. We only selected the comets from which we had both the outgassing rate and the heliocentric distance (between the object and the Sun).
In the dataset, we opted to use data corresponding to values obtained at two different locations along the comet's trajectory and created a dataset of outgassing rate and heliocentric distance at perihelion and the ascending node (see *Appendix 3: Illustration showing the main orbital elements in space*).

We were left with 29 comets out of which 26 had outgassing rates values both at the perihelion and at the ascending node. Then, we only selected the comets which have distances at the ascending node inside of 4 AU, to finally arrive at a 19 comets dataset.

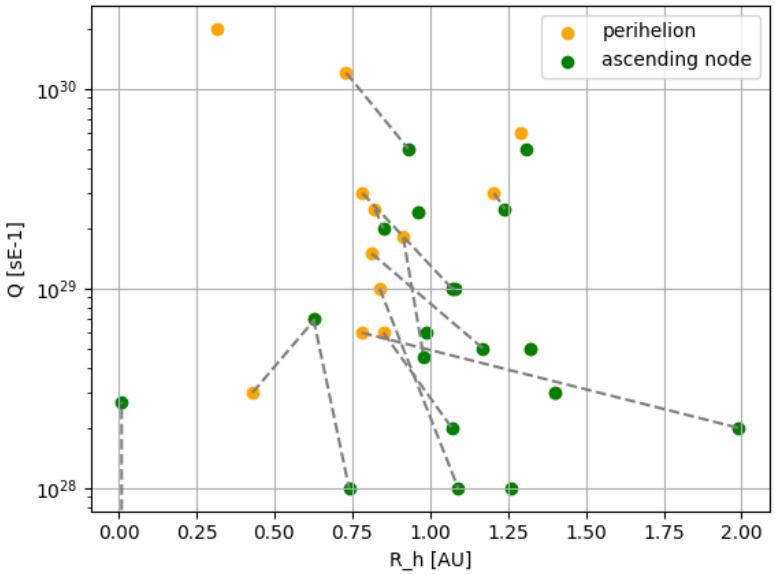

Figure 2: Outgassing rate versus the heliocentric distance for the comets shortlisted in the study. For most comets, the outgassing rates are determined at both perihelion and the ascending node with a dashed line connecting them

Fig.2 shows the outgassing rate at the perihelion (orange dots) and at the ascending

node (green dots) for the 19 comets. For each comets, the two data points are linked by a grey dashed line.

The comets composing our samples have heliocentric distances ranging from 0.1 to 2 AU, and outgassing rates ranging mainly from 10^{28} to 10^{31} s^{-1}. According to the classification of comet outgassing rates by Götz et al. (2022), our two samples contain comets with very active outgassing rates, compared to comet 67P. This is highly beneficial for Comet Interceptor considering that we have yet to identify the specific comet for study, and most instruments get more insteresting data from a very active comet.

Moreover, we can see that the slopes linking the dots coming from the same comets are mostly decreasing from the perihelion to the ascending node; the perihelion being the closer point with the Sun on the comet trajectory, this Figure 2 agree with the expectation of lower activity far from the Sun.

RESEARCH PROJECT : MODELING THE POSITION OF MAIN COMETARY PLASMA BOUNDARIES

The modeling of cometary plasma environments, or more specifically the dynamic regions where particles released by comet nucleus interact with the solar wind is the main emphasis of this study. Our study is around this intricate interaction between comet particles and the solar wind, which helps us understand comet dynamics and how they affect their spatial surroundings. This modeling work has an importance in elucidating the underlying mechanisms of these phenomena and paves the way for a better understanding of the cometary plasma environments and for the planning of Comet Interceptor operations.

A. THE BOW SHOCK LOCALISATION

1. Calculation of the stand-off distance of the bow shock with the model

a. The stand-off distance of the bow shock model

Given the outgassing rates and heliocentric distances mentioned in the last paragraph, we calculated the stand-off distance of the bow shock generated in front of the comets (i.e distance along the comet-Sun line) at that specific heliocentric location, using a formula provided by Koenders et al. (2013) and validated by Edberg et al. (2024). This model describes 1D inviscid gas flow without the effects of the magnetic field in a stationary situation upstream the bow shock. This means that it considers only a mass source interacting with a fluid.
The stand-off distance of the bow shock ($R_{BS,K}$) for a given outgassing rate (Q) is given by:

$$R_{BS,K} = \frac{v_n Q m_i}{4\pi u_n n_{sw} m_{sw} u_{sw}((\rho u_x)^*_{crit} - 1 + A)} - R_s \quad \text{(Eq. 2)}$$

$$\text{With } A = \frac{v_n Q m_i}{4\pi u_n n_{sw} m_{sw} u_{sw}(\frac{u_n}{v_n} + R_n)} \quad \text{(Eq. 3)}$$

$$R_s = \frac{u_{sw}}{\Omega_{ci}} * (\Omega_{ci} t_p - \sin(\Omega_{ci} t_p)) \quad \text{(Eq. 4)}$$

$$\Omega_{ci} = \frac{q_e * b_{sw}}{m_i} \qquad \text{(Eq. 5)}$$

where v_n is the total ionisation rate, Q the outgassing rate, m_i the mass of the cometary ions, u_n the neutral velocity, n_{sw} the solar wind density, m_{sw} the mass of the solar wind protons, u_{sw} the solar wind velocity, Ω_{ci} the ion gyrofrequency, and $(\rho u_x)^*_{crit}$ the critical value of the normalized mass flux density. The term A used in Eq.2 and defined in Eq. 3 comes into play for high outgassing rates, and limited ion-mass source, which leads to that the maximum distance of the interaction region will be dictated by the ratio between the ionisation rate (ν) and the neutral flow velocity (u_n/ν). Beyond this distance, the plasma mass-flow will be so limited that it cannot withhold the incoming solar wind any longer. The R_s term used in Eq. 2 and defined in Eq. 4 takes into account the time ions need to be picked up by the solar wind, accelerated from the instant they where ionized.
The parameters in Eq 2-5 are explained in Table 1 below along with typical values at 1AU.

Table 1: parameters at 1 AU

Parameter	Name	Value	Unit
v_n	Total ionisation rate	$7x10^{-7}$	s^{-1}
m_i	Mass of the cometary ions	$17 * 1.66x10^{-27}$	kg
u_n	Neutral velocity	$6x10^{2}$	$m.s^{-1}$
n_{sw}	Solar wind density	$5x10^{6}$	m^{-3}
m_{sw}	Mass of the solar wind ions (protons)	$1 * 1.66x10^{-27}$	kg
u_{sw}	Solar wind velocity	$400x10^{3}$	$m.s^{-1}$
ρu_x	Critical value of the normalized mass flux density	1.3	Ø
R_n	Radius of the comet nucleus	2000	m
q_e	Elementary charge	$1.602*10^{-19}$	C
$\Omega_{ci}t_p$	Ø	$2\pi * 0.216$	Ø
b_{sw}	Solar wind magnetic field strength	10^{-9}	T

b. Scaling the parameters

The parameters given in Table 1 are for an heliocentric distance of 1 AU and some of the parameters scale with R_h. Indeed, the total ionisation rate (ν_n), the solar wind density (n_{sw}), the neutral velocity (u_n), and the magnetic field (B_{sw}) need to be rescaled as they vary with this distance. Therefore, we cannot directly use the values given in Table 1, which are taken at 1 AU and must use their actual values based on the actual heliocentric distance. We utilized the following relations

$$n_{sw,r_h} = \frac{n_{sw}}{r_h^2} \quad \text{(Eq. 6)}$$

$$\nu_{r_h} = \frac{\nu_n}{r_h^2} \quad \text{(Eq. 7)}$$

$$u_{r_h} = \frac{u_n}{r_h^{0.5}} \quad \text{(Eq. 8)}$$

The solar wind density expends spherically with the solar wind and therefore scales as $\frac{1}{r_h^2}$ (Cochran & Schleicher, 1993) with heliocentric distance (Eq. 6), the ionisation frequency depends on solar illumination which also decreases with heliocentric distance as $\frac{1}{r_h^2}$ (Eq. 7), while u_n falls off as $\frac{1}{r_h^{0.5}}$ (Eq. 8) as suggested by Cochran & Schleicher (1993). We also use

$$\Omega_{ci,r_h} = \frac{\Omega_{ci} * b_{sw,r_h}}{m_i} \quad \text{(Eq. 9)}$$

Where $b_{sw,r_h} = \frac{b_{sw}}{(1+r_h^2)^{0.5}} * r_h^2$ (Eq. 10) and $\Omega_{ci,r_h} * t_{p,r_h} = 2 * \pi * 0{,}216$ (Eq. 11), which can be directly incorporated in the Eq. 4.

The stand-off distance of the bow shock as a function of the heliocentric distance is depicted in Figure 3, and as a function of the comets' outgassing rate in Figure 4. It is noted that the bow shock typically occurs between 10^4 and 10^6 km.
In Figure 3 and Figure 4, we can see that for the same comet (two pairs for dots linked with the dotted grey line), the stand-off distance is mostly higher at the perihelion, giving us mostly negative slopes for Figure 3, and positive slopes for Figure 4.

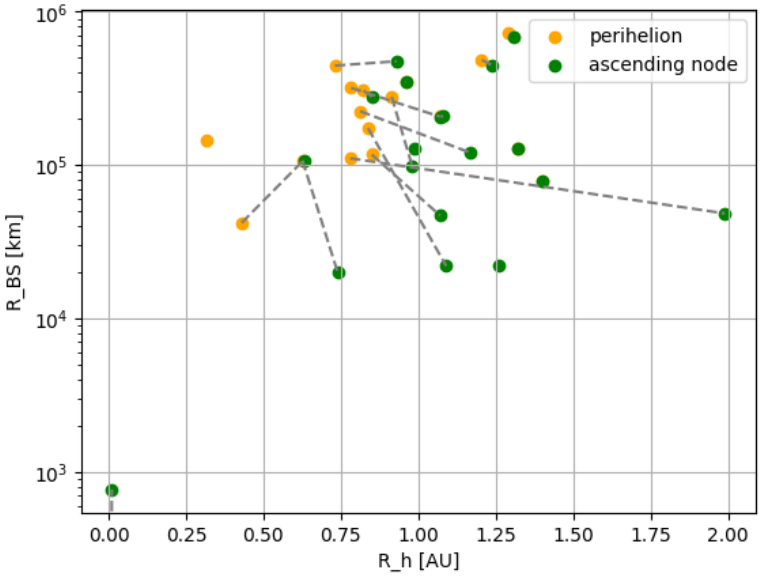

Figure 3: Stand-off distance of the bow shock versus heliocentric distance for the two samples considered in this study, associated to selected comets perihelion and ascending node. Two dots coming from the same comet are linked with a grey dotted line

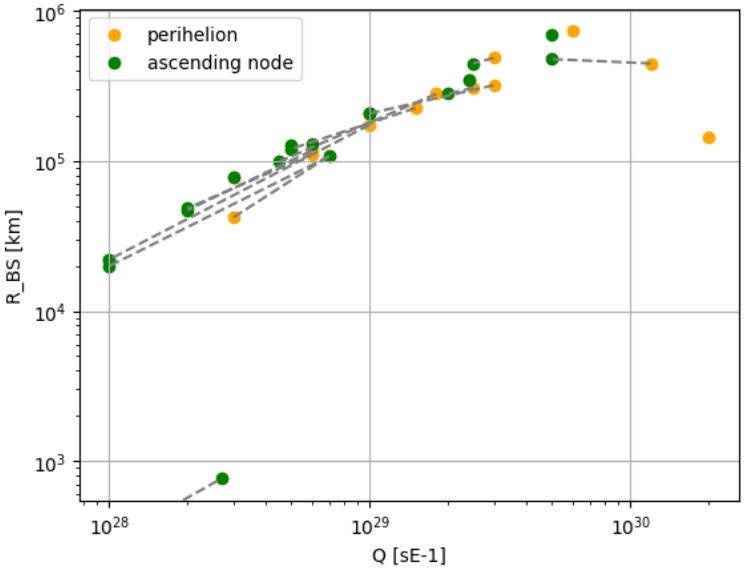

Figure 4: Stand-off distance of the bow shock versus outgassing rate for the two samples considered in this study, associated to selected comets perihelion and ascending node. Two dots coming from the same comet are linked with a grey dotted line

Furthermore, the outgassing rate also varies with heliocentric distance, but its scaling law is more complex, and different for every comet. It is imperative for us to seek how to constrain this dependence of the outgassing rate on the heliocentric distance.This rescaling is not necessary for the real measured values, i.e., those from the list of comets we are studying. However, for the model, it is necessary to account for the fact that the outgassing rate also varies with heliocentric distance, which is more difficult to constrain than the other parameters. Its expression is given by (see Jewitt, 2022):

$$Q(r) = aQ_{1AU} * ((\frac{r}{r_0})^b * (1 + (\frac{r}{r_0})^c))^d \qquad \text{(Eq. 12)}$$

With Q_{1AU} the outgassing rate at 1 AU in s^{-1}, and r the heliocentric distance in AU. The value of the five other parameters can be found in Table 2 below.

Table 2 : parameters used in Eq. 12

Parameter	Value	Unit
a	0.111262	-
b	-2.15	-
c	5.093	-
d	-4.6142	-
r_0	2.808	AU

The objective here is to plot the stand-off distance of the bow shock versus the heliocentric distance of the comet, for different values of outgassing rate, to understand how the extent of the bow shock change with both parameters.

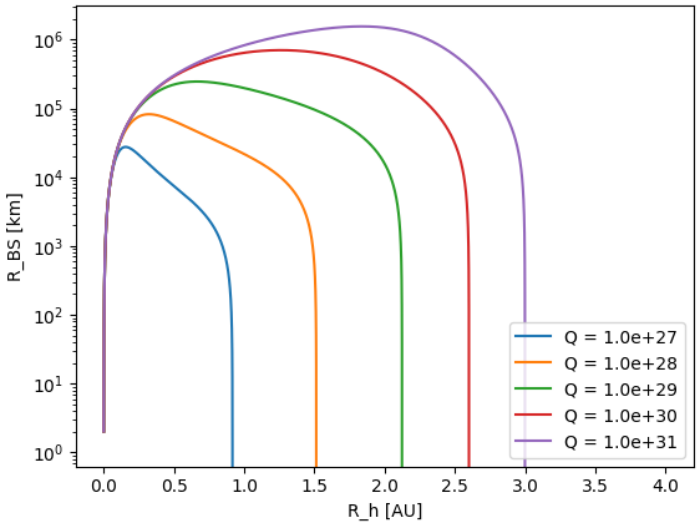

Figure 5: The stand-off distance of the bow shock versus the heliocentric distance, from the model described by Eq. 2 and with parameters scaled according to Eq. 6-12. This model is evaluated for different outgassing rates at 1 AU

Figure 5 shows the bow shock distance as a function of the heliocentric distance, for five different values of outgassing rates at 1 AU, from 10^{27} to 10^{31} s^{-1}.

For these five outgassing rates, the curves overlap and increase up to a bow shock distance value of approximately 10^4 km at Rh = 0.2 AU before separating. This bow shock value peaks for Q = 10^{27} s^{-1}, which is the smallest outgassing rate in our figure, at around 0.1 AU.

For the other four outgassing rates, which are higher than this, their curves continue to progress until they reach their respective maxima, and then decrease sharply. The higher the outgassing rate, the higher the maximum value of their curve is, meaning the maximum value of their stand-off distance of the bow shock will also be larger. In other words, two comets at the same distance from the Sun on their trajectory will have different stand-off distances of the bow shocks, which will depend on their outgassing rates. The higher the rate, the larger the bow shock is. All five curves follow this pattern, and this figure clearly shows that the outgassing rate has a significant effect on the bow shock and cannot be constrained only by considering the heliocentric distance, as it has been done with the rescaling of parameters (see section 2.b. above).

2. Compare the data with 67P and Hale Bopp

Now that we have data coming from both measurements and model, a next objective was to compare our selected dataset with other broader studies. We only have one dataframe containing two datasets of comets (first data taken at the perihelion and second the ones taken at their ascending node), each containing 19 comets. Therefore, it's interesting to see if our results align with those of other studies on a larger scale. We were particularly interested in the study by Hansen et al. (2016), which studied the evolution of the H_2O outgassing rate of Comet 67P using data collected during the Rosetta space mission. Comet Hale Bopp is one of the most active comets ever observed and it also included as to get an upper limit of what we could expect; its data were included using Colom et al. (1997). This comparison helps us understand whether our results are consistent with those obtained from a more extensive dataset and from a well-studied comet like 67P.

In Hansen et al. (2016), the outgassing rate was presented as a function of heliocentric distance. We aimed to replicate this figure for our study.
To achieve this, the data we needed (heliocentric distance, cometocentric distance and density) was obtained from the AMDA database (https://amda.irap.omp.eu/), and insert in a simple version of the Haser model (Eq. 1) providing the outgassing rate Q, related to the neutral density n, at cometocentric distance r_c according to

$$Q = 4\pi n r_c^2 v_n \qquad \text{(Eq. 13)}$$

where n is the neutral gas density, and v_n is the neutral expension velocity. We sought to enhance the analysis of our thesis by generating results that were in line with Hansen's findings by adding these parameters and applying the procedure. The Hale Bopp data were extracted from Fig. 3 in Colom et al. (1997) directly.

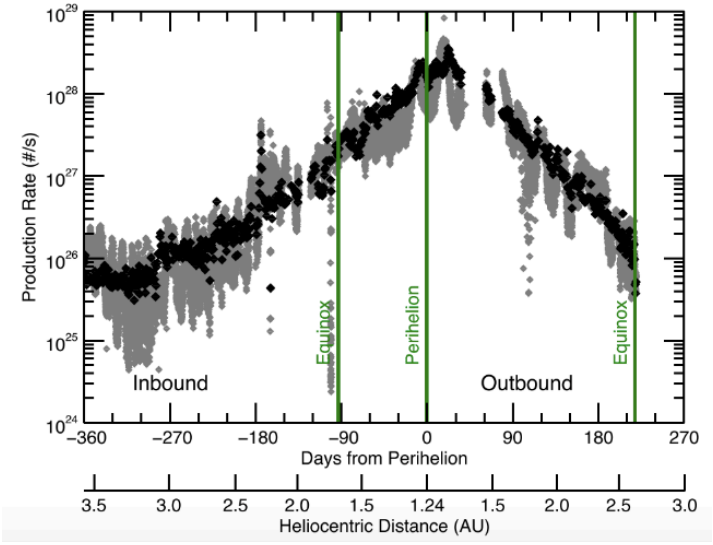

Figure 6: 67/P outgassing rate versus the heliocentric distance from Hansen et al. (2016)

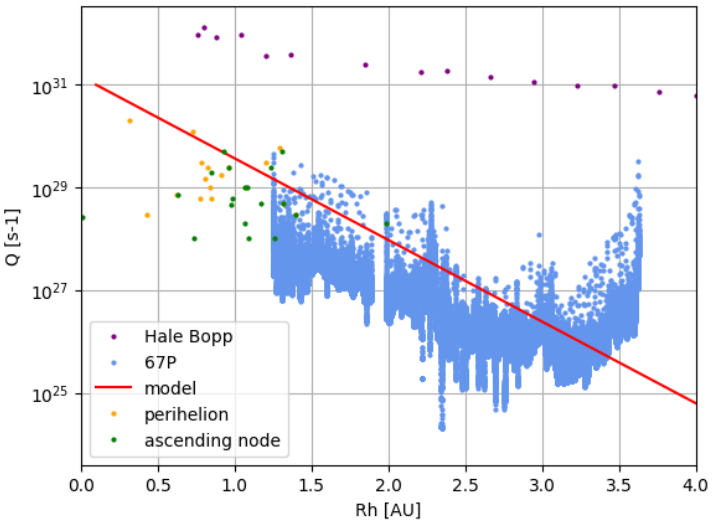

Figure 7: Outgassing versus the heliocentric distance for the selected dataset used in the study, 67P and the Hale Bopp comet. Data from Rosetta outside of 3 AU is uncertain

We have reproduced the outgassing rate from 67P in Figure 7, and compared that to Figure 6 from Hansen et al. (2016). Only the outbound phase of the comet was plotted, specifically referring to its trajectory after perihelion (around 1.24 AU) when it is moving away from the Sun.
This decreasing trend is normal and expected because, during this part of the trajectory, as the comet moves away from the Sun, it outgasses less and less.

In addition, we generated random outgassing rate and heliocentric distance data to calculate the red line, and depict the theoretical behavior of the comets from the selected dataset and of 67P/Churyumov-Gerasimenko. It is clear that the data fits well with the model. Lastly, we have also plotted the Hale-Bopp in purple. As be seen, Hale-Bopp exhibits the behavior of the model but at a slower rate of decrease. Additionally, it has several orders of magnitude higher values than our data and the model, which is a consequence of its extremely high activity at such low heliocentric distances.

Given the known heliocentric and cometocentric distances of comet 67P, we were able to plot the Rosetta spacecraft's trajectory in Figure 8 and overlay its stand-off distance from the bow shock.

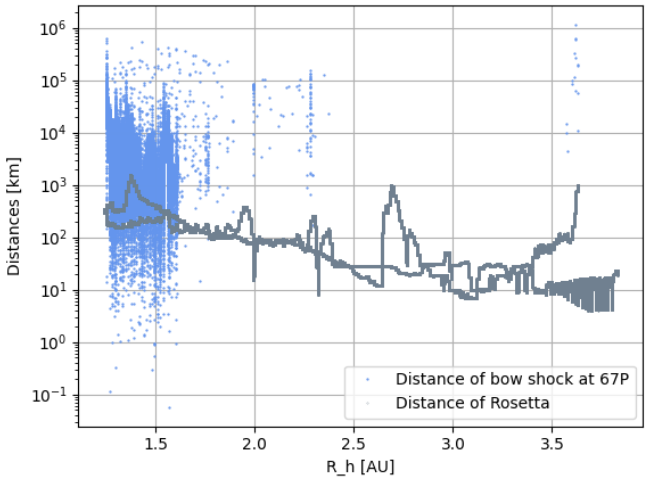

Figure 8: Rosetta trajectory compared to the stand-off distance of the 67P bow shock versus its heliocentric distance. Note that the distance of Rosetta is not in the subsolar direction

Figure 8 illustrates whether or not the Rosetta spacecraft crossed comet 67P's bow shock during its operational period. The x-axis represents the heliocentric distance, while the y-axis represents the cometocentric distance (i.e., the distance from the comet's nucleus) of both 67P's bow shock (depicted in sky blue) and Rosetta (depicted in grey).

The calculated bow shock stand-off distance vary and sometimes fall below the cometocentric distance of Rosetta, indicate the possibility of crossing. This could occur either because Rosetta crosses the bow shock or the bow shock moves past Rosetta, which seems a more likely scenario given Rosetta's slow relative speed of 1 $m.s^{-1}$. Significant interactions and observations of the bow shock are likely when the heliocentric distance of 67P is less than 1.6 AU. This is when the bow shock can extend far enough from the comet nucleus to intersect with Rosetta's trajectory, and so Rosetta should have crossed the bow shock around 1.6 AU, so next to 67P's perihelion.

a. Stand-off distance of the bow shock vs the heliocentric distance

In Figure 9 we show the bow shock distance as a function of heliocentric distance. This figure allows us to compare the stand-off distance of the bow shock values for the comets from the selected dataset for this study, with 67P and Hale Bopp.

To achieve this, we utilized the data from Hansen et al. (2016) for 67P as well as the ones from Colom et al. (1997) for Hale Bopp to plot the previous Fig. 7, along with the bow shock results we calculated. Instead of plotting the heliocentric distance against the outgassing rate, we plotted them versus the bow shock distance. This approach offers us a fresh perspective on the interactions between the solar wind and the celestial bodies under study, by comparing data and exploring variations with respect to distance from the Sun. It also allows us to see how far out the bow shock was of comet 67P when Rosetta was orbiting the comet close to the nucleous (within 1500 km, but mostly at a few 100's of km).

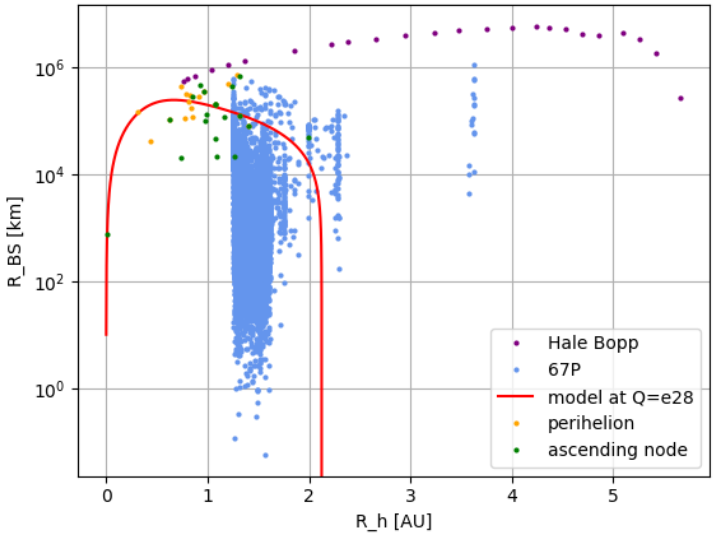

Figure 9: Bow shock distance versus the heliocentric distance for the selected dataset used in the study, 67P and the Hale Bopp comet

The model's predicted behavior for the values has been illustrated by the theoretical red line (at $Q = 10^{28}$ s^{-1} because it is the best fit) next to our data (at perihelion in orange and at the ascending node in green). Furthermore, we have added the data from the Hale-Bopp comet in purple and the ones from Hansen et al. (2016) relative to 67P in light blue.

As seen in Figure 9, there is a significant amount of overlap and strong correlation between the selected dataset and the data used by Hansen et al. (2016), which corresponds to the upper section of the theoretical curve. Furthermore, because of its great activity at such a little distance from the Sun, the Hale Bopp data are still higher than all the other ones.

b. Stand-off distance of the bow shock vs the outgassing rate

The stand-off distance of the bow shock were then plotted against the outgassing rate, in order to understand if this factor has an impact on this distance.

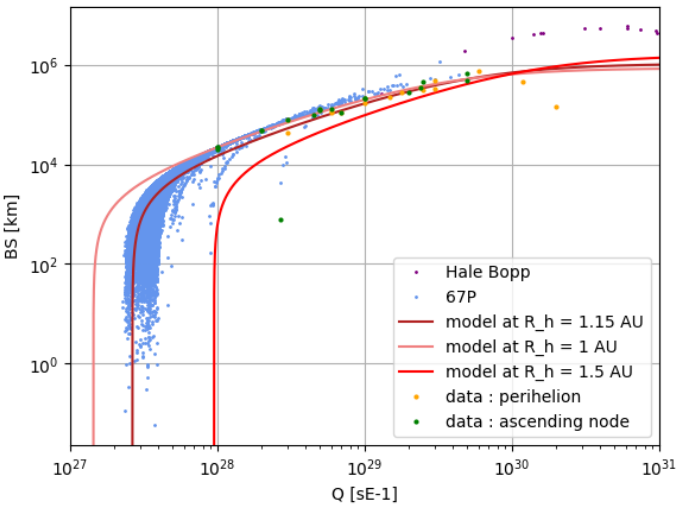

Figure 10: Bow shock distance versus the outgassing rate for the selected dataset used in the study, 67/P and the Hale Bopp comet

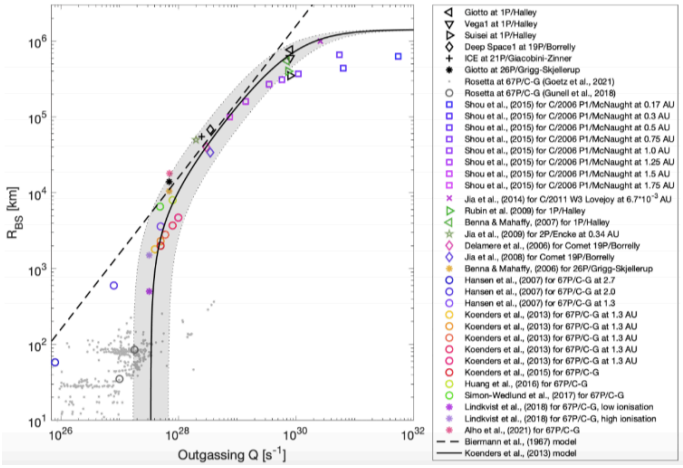

Figure 11: Subsolar stand-off distances of bow shocks from previous cometary flyby missions as well as from simulations of solar wind-comet interactions from Edberg et al. (2024)

Here again in Figure 10, our data agrees well with Hansen et al. (2016) results as well as the theoretical predictions (at R_h = 1 AU, 1.2 AU and 2 AU). The overall pattern and coherence with Hansen et al. (2016) data and the theoretical model maintain the validity of our findings in the context of the theoretical predictions and previous research. The 67P (in light blue), the selected dataset we used for the study (in orange for data at perihelion, and in green for the ones at the ascendant node), and Hale-Bopp (in purple) were added once more to the figure. As can be seen, they as well coincide with the model.

That Figure 10 can be compared with Figure 11 from Edberg et al. (2024) information from earlier research and other models, were assembled. When we compare Figures 10 and 11 together, we can see that the patterns and values found in our research match both historical data and Edberg et al. (2024) theoretical theories. In addition to the known values of comets that have been previously investigated, Edberg included in his figure the various

theoretical frameworks that have been employed to analyze the bow shock's behavior. This thorough compilation offers a solid basis for validation of our findings. When compared to Figure 11, comets from our selected dataset show a good agreement with the overall patterns and expected behaviors.

To summarize, the analysis of Figures 10 and 11 shows that our model and observations are in good agreement with the accepted values and patterns found in the scientific literature. This uniformity adds credence to our findings and implies that the events we studied align well with what is currently known about bow shock dynamics around comets. However, The Hale Bopp data seems to still be higher than the model.

B. THE DIAMAGNETIC CAVITY & EXOBASE LOCALISATIONS

1. The diamagnetic cavity position

The diamagnetic cavity is the second important boundary that the solar wind ions meet as they travel closer to the comet's nucelus after the bow shock. This cavity can be described as the region where the magnetic field is either completely missing or drastically reduced. The diamagnetic cavity forms because the strong interaction between the solar wind and the comet's own outgassing. The outgassing creates a region of plasma around the nucleus. The interaction between the solar wind and this plasma induces a magnetic field, but the resulting magnetic pressure and field lines are compressed or redirected away from the comet's nucleus.
Simply the diamagnetic cavity is a region where the strong plasma environment leads the magnetic fields to be suppressed.

In Cravens et al. (1987), the position of the diamagnetic cavity ($R_{DiamagneticCavity}$) can be calculated from the outgassing rate of the comets according to:

$$R_{DiamagneticCavity} = \frac{Q^{\frac{3}{4}}}{B_{cavity}} * c \quad \text{(Eq.14)}$$

With Q the outgassing rate in $mol.s^{-1}$, B_{cavity} the magnetic field strength in the pile-up region in nT and $c = 7{,}08 \times 10^{-18}$ $km.nT.s^{3/4}$. For this study, the magnetic field was fixed at $B_{cavity} = 50$ nT.

Equation 14 assumes that the ions are formed from H2O by photoionization or electron impact ionization which is not the case in reality, however this model will allow a better understanding of the diamagnetic positions of the comets we are interested in this study.

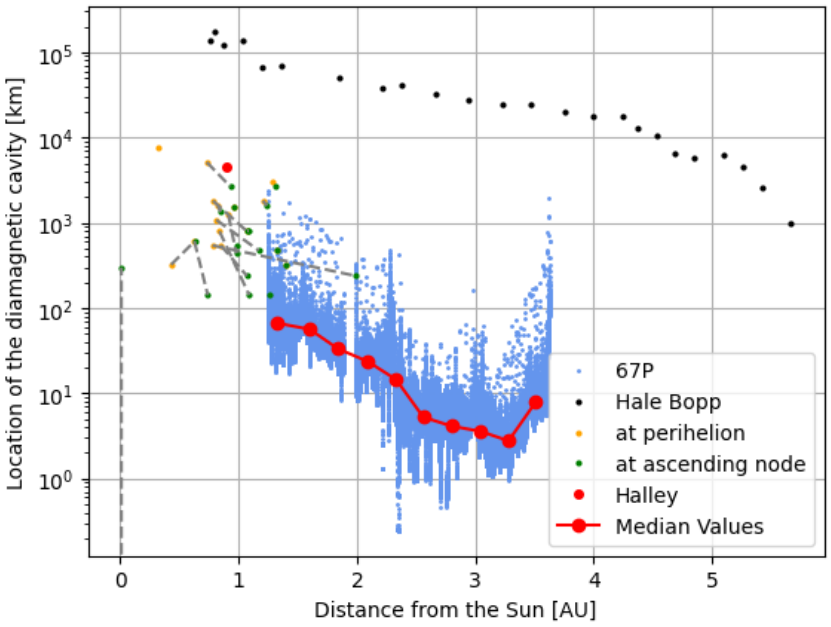

Figure 12: Diamagnetic cavity position versus the heliocentric distance for the selected dataset used in the study, 67/P and the Halley comet

On Figure 12, the position of the diamagnetic cavity is shown in function of the heliocentric distance for the objects we are studying : 67P, Hale Bopp and the selected dataset of 19 comets that could have been Comet Interceptor targets. We also added the data for the Halley comet in red for which only one outgassing rate and heliocentric distance are known at one place thanks to an observation. Also, the median values of 67P were added in red to better read the figure and the pattern.
On that figure, the comets coming from the selected dataset, Halley and 67P agree together and show that the closer the comet is to the Sun, the bigger its diamagnetic cavity will be. Noteworthy, Hale-Bopp also agrees with this trend but is found at much larger distances due to its intense activity.

2. The exobase localisation

After traveling through the diamagnetic cavity and the bow shocks, we can approach the comet's nucleus and cross another significant barrier, the exobase. This boundary is defined by the exopause, which serves as a separation between two distinct zones around the comet. The environment is sufficiently dense inside the exopause allowing ion collisions to occur frequently and with considerable impact. This region is close enough to the comet's nucleus that the interaction between the comet's outgassed material and the surrounding space environment influences the behavior of ions and other particles. The particle density rapidly increases within the exopause, and the low density of matter outside of the exopause causes ions to collide less often; there are fewer interaction in this outer region.

To calculate the exobase position ($R_{exobase}$) of the comets, we used a model computed by Henri et al. (2017) and given by : $$R_{exobase} = \frac{Q * \sigma_{en}}{4\pi * u_n}$$ (Eq.15)

with $R_{exobase}$ in m.
Q is the outgassing rate in s^{-1}, σ_{en} = 5x10^{-20} m^2 the electron-neutral cross-section and u_n = 10^3 $m.s^{-1}$ the neutral velocity.

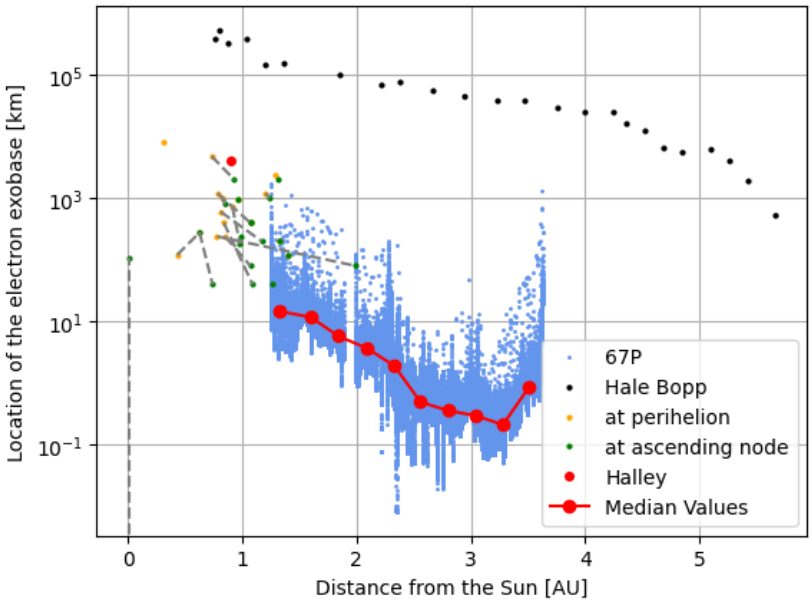

Figure 13: Exobase location versus the heliocentric distance for the selected dataset used in the study, 67/P and the Halley comet

Figure 13 can be compared with fig. 12 because of the data coming from all the comets seem to have the same scales and way of decreasing.

3. Compare the diamagnetic cavity and exobase localisations

On Figure 14, only the comets coming from the selected dataset are displayed. The figure show the location of both the bounderies as function of the heliocentric distance. The exobase locations of all the 19 comets are shown each by a dot while their diamagnetic localisations are marked by a cross.

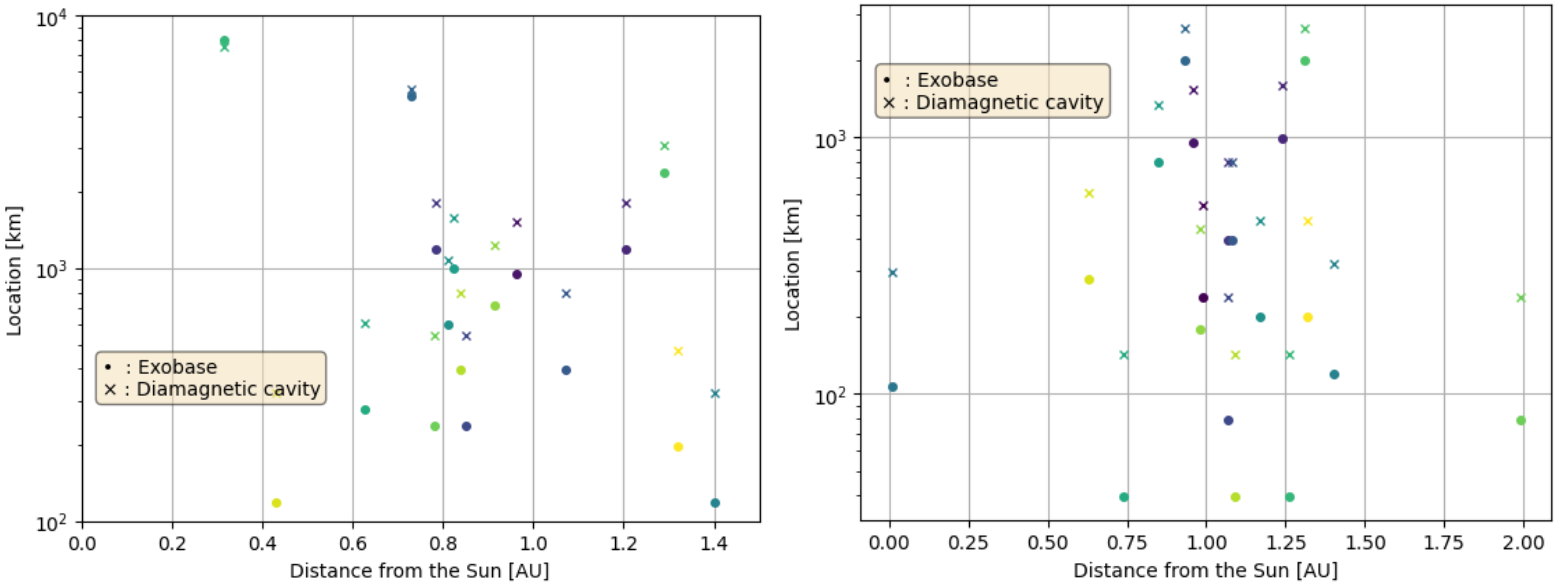

Figure 14: Diamagnetic cavity and exobase locations versus the heliocentric distance for the selected dataset. Data coming from the perihelions are shown on the left figure while the ones coming from the ascending nodes are shown on the right one

First, we can see that for each pair of comet, both the diamagnetic cavity and exobase are located exactly on the same distance from the Sun which is expected as the bounderies were calculated at the same heliocentric distances, however we can note that of most of the comets, the diamagnetic cavity do have a higher size. Indeed, the crosses (the diamagnetic cavities) are displayed above the dots (the exobases), which is also expected as the diamagnetic cavity is the first boundary that the spacecraft travelling to the comet nucleus can cross, right after the bow shock, and just before the exobase.
Moreover, they all have different size, bigger for the diamagnatic cavity, but all have sizes between 10^2 and 10^4 km, exept for the data on the right figure (the ones taken at ascending node) which can have exobase under 10^2 km.

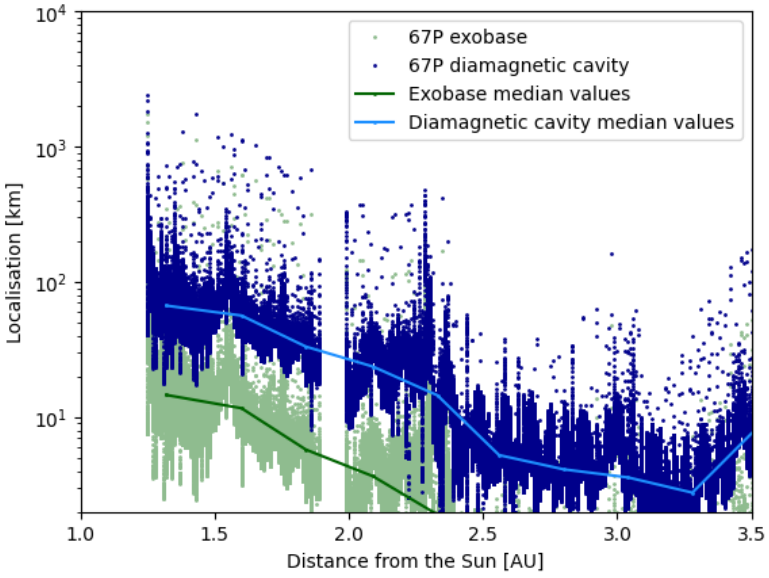

Figure 15: 67P diamagnetic cavity and exobase locations versus its heliocentric distance

We reproduced the work on 67P to see the difference between 67P diamagnetic cavity and its exobase location on fig.15. The figure was cut at a minimum location of 2 km which correspond at 67P radius.
Once again, the two boundaries follow the same pattern and have a different order of magnitude; the exobase location is always under the diamagnetic cavity one with a factor of approximatively 100 km. The higest values can be relevated at a distance from the Sun of 1.4 AU, which is the perihelion from 67P on its trajectory; this is in coherence with the results from this study as at the perihelion, 67P has the highest outgassing rate on which the the diamagnetic cavity and the exobase locations depend directly and proportionnaly .

As explained at the beginning of the report, the boundary positions at comet 67P were calculated based on the neutral density and cometocentric distances, derived from the data provided by Hansen et al. (2016).
After having those figures, the next step was to use the time and positions of when Rosetta was actually observed to cross these boundaries, as seen in time series of data and previouslty published. We use those files here. The goal was to extract these real crossing times and compare them with the positional data. This allows us to determine the exact positions (both heliocentric and cometocentric) of the spacecraft at the time of each crossing. Having this exact positions and time of crossing, the outgassing rates associated were calculated using Eq. 13 from Hansen et al. (2016), then the location of the diamagnectic cavity and exobase using Eq. 14 and Eq. 15 by fixing the neutral density at u_n = 1.9x10^7 cm^{-3}, corresponding to the mean density of that interval.

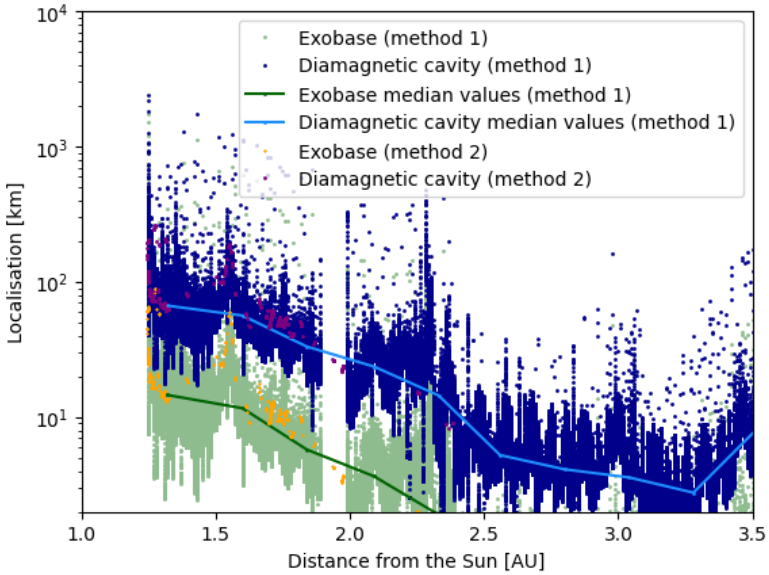

Figure 16: 67P diamagnetic cavity and exobase locations versus its heliocentric distance corresponding to the data from Hansen et al. (2016) (method 1) and the ones taken at the actual time where Rosetta crossed its diamagnatic cavity (method 2)

On Fig. 16, the data coming from Hansen et al. (2016) are called with the legend as « Method 1 » while the ones coming from the actual observed crossings are refered as « Method 2 ». It is pretty obvious that all the data superpose and agree with each other, meanning that the actual 67P data (positions and time of crossing the diamagnetic cavity) allow to have the same size and locations of its exobase and diamagnetic cavity as the first attempt with the 67P data coming from Hansen et al. (2016). The first method is using more

than a million data points while the second method refers to a file where 713 real crossing are indicated.

CONCLUSION & PERSPECTIVES

The primary objective of the project was to model the cometary plasma environment to prepare for the Comet Interceptor mission. The main focuse was the stand-off distance of bow shock for a selection of comets, coming from a list of historical comets that could have been reachable if Comet Interceptor would have been already launched. The list was compiled by the Comet Interceptor project team.
The relations between the bow shock distance with the heliocentric distance and the outgassing rate were examined and, we also compared the selected dataset with well-known comets 67P/Churyumov-Gerasimenko and Hale-Bopp.
Additionally, the Rosetta trajectory was inspected in order to understand if the spacecraft crossed 67P bow shock boundary during its operation. The link between heliocentric and cometocentric distances is illustrated graphically in Fig. 8, making it possible to see when the spacecraft was in a favorable position to see the bow shock. These data are crucial for understanding the dynamic interactions between the comet and the solar wind, especially as comet 67P approaches within 1.6 AU of the Sun, a period when the bow shock can extend sufficiently to intersect Rosetta's trajectory.

The model from Koenders et al. (2013) was used to calculate the stand-off distance of each comet's bow shock, utilizing a selected dataset that included the necessary outgassing rates and heliocentric distances. Parameters were rescaled to ensure they varied in accordance with the heliocentric distance, such as the outgassing rates in the theoritical model.

Our findings indicate that the stand-off distance of the bow shock is dependent on the heliocentric distance up to approximately 2 AU for 67P and the selected dataset. Beyond this heliocentric distance the bow shock simply did not form due to the low outgassing rate. However, this relationship does not hold for Hale-Bopp due to its exceptionally intense plasma activity. Additionally, the stand-off distance rises in direct proportion to the outgassing

rate. The Comet Interceptor mission may be impacted by these findings. Thank to the results, European Space Agency (ESA) could make important plans for the space mission, and scientists could estimate the outgassing rate and calculate the stand-off distance of the bow shock by knowing the target's heliocentric distance. If it is desired to cross the boundary of the bow shock, this knowledge is essential for determining where this will happen.

The second phase of this master's thesis involves meeting with co-supervisor Pierre HENRI in Nice Observatory, in order to study another cometary boundary: the diamaganetic cavity, a region where the magnetic field is excluded because of the comet's outgassing, and remains at that time poorly understood and inadequately described. Another boundary has been studied at the same time, the exobase, which is the region delimiting the region where particules can enter in collision (outside the exobase) with the region where those collisions become negligeable (inside the exobase); the exobase represent the limit between the dense lower atmosphere to the more tenuous exosphere around a comet nucleus.

The previous study on the bow shock was expanded in order to calculate the diamagnetic cavity and the exobase position on the very same comets: the selected dataset of the 19 comets, Hale Bopp and 67P. The same models were used to calculate the outgassing rate of this comets in order to be able to calculate the location of the diamagnetic cavity with the Cravens et al. (1987), and the location of the exobase with the Henri et al. (2017).

The results show that the location of both the diamagnetic cavity and the exobase location depend of the heliocentric distance of the comets.
Comets from the selected dataset do have a small size difference between the diamagnetic cavity and exobase (100 km at a maximum) while the 67P does see a strong size difference between them: at the perihelion (around 1.4 AU), the diamagnetic cavity does have a size of 100 km while its exobase does have one around 10 km, which is a factor 10. Hale Bopp is, once again, considered as the upper limit for which a difference between the location of the both bouderies cannot be seen; the size of the diamagnetic cavity and the exobase appear to be similar in our study and around 10^5 km at the maximum. Once again, the Comet Interceptor mission may be impacted by these findings and cross both the diamagnetic cavity and the exobase of the selected comet if it is close enough to the nucleus, at around 10^3 km, at 1 AU from the Sun.

Studying all the bow shock, the diamagnetic cavity and the exobase not only help for Comet Interceptor, but also add knowledge regarding boundaries, and improve our general understanding of cometary plasma environments.

ACKNOWLEDGMENT

Before beginning, it was important for me to acknowledge the people who supported me during the master's thesis, and before, when it was only a dream, then became a project.

First of all, I would like to thank Niklas EDBERG, scientist and my supervisor during this project. Indeed, from the beginning he trusted me and allowed me to join him for this wonderful master's thesis, that he thought about for me, after I told him what I wanted to study the first time we met. During all the time the placement took place, he has been very positive, helpful, comprehensive and patient with me, and offered me such a wonderful opportunity, a life experience, by inviting me to a group meeting in Björkliden, Lapland, where I could meet people from different countries who work on comets.

I also want to thank Erik VIGREN and Anders ERIKSSON, scientists and also the co-responsive of my project, for being here each time I needed to ask questions, and feedback on my work in progress. I also want to give a special acknowledgment to Pierre HENRI, a scientist and also co-responsive of the project, for his collaboration on my project, his pieces of advice and his caring since the day I met him in the meeting in Lapland. Moreover, he invited me to spend a week with him in his lab in Nice (FRANCE) to open, link and enriching the project with his ongoing activities, and for me to have a real co-supervised experience.

Moreover, I would like to thank the team at the IRF Uppsala, the scientists as well as the engineers, Ph.D. students and interns, for making me feel welcome since the first day, and for all the moments we shared together ; the project isn't finished yet, I am happy to have more time to spend with all these wonderful people, who became friends for some of them.
A special thank you will also go to Lina HADID, my teacher in Plasma Physics, for giving me this deep interest in this field during the lessons, and for giving me contacts and tips to pursue my wish to realize my master's thesis in Sweden.

To conclude, I would like to thank my friends and family who believed in the project, followed my adventures, and the ones who came to visit me during this first 4 months in Sweden.
My last words will be for my life partner, who decided to leave his family and everything he knows to come living in Sweden with me ; nothing would have been possible without him.

REFERENCES

Bailer-Jones, C. A. L., Farnocchia, D., Ye, Q., Meech, K. J., & Micheli, M. (2020). A search for the origin of the interstellar comet 2I/Borisov. *Astronomy & Astrophysics*, *634*, A14. https:/doi.org/10.1051/0004-6361/201937231

Brooke, T. (1997). Endeavour, vol. 21, issue 3, pages 101-104. Elsevier

Cochran, A. L., & Schleicher, D. G. (1993). Observational Constraints on the Lifetime of Cometary H2O. *Icarus*, *105*(1), 235–253. https://doi.org/10.1006/icar.1993.1121

Colom, P., Gérard, E., Crovisier, J. *et al.* Observations of the OH Radical in Comet C/1995 O1 (Hale-Bopp) with the Nançay Radio Telescope. *Earth, Moon, and Planets* 78, 37–43 (1997). https://doi.org/10.1023/A:1006206924786

Cravens … 1987

Crovisier, J., Colom, P., Gérard, É., Bockelée-Morvan, D., & Bourgois, G. (2002). Observations at Nançay of the OH 18-cm lines in comets. *Astronomy Astrophysics*, *393*(3), 1053–1064. https://doi.org/10.1051/0004-6361:20020673

Davidsson, B. J. R., Sierks, H., Güttler, C., Marzari, F., Pajola, M., Rickman, H., A'Hearn, M. F., Auger, A., El-Maarry, M. R., Fornasier, S., Gutiérrez, P. J., Keller, H. U., Massironi, M., Snodgrass, C., Vincent, J., Barbieri, C., Lamy, P. L., Rodrigo, R., Koschny, D.,. . . Tubiana, C. (2016). The primordial nucleus of comet 67P/Churyumov-Gerasimenko. *Astronomy & Astrophysics*, *592*, A63. https://doi.org/10.1051/0004-6361/201526968

Edberg, N. J. T., Eriksson, A., Vigren, E., Nilsson, H., Gunell, H., Götz, C., Richter, I., Henri, P., & De Keyser, J. (2024). Scale size of cometary bow shocks. *Astronomy & Astrophysics*, *682*, A51. https://doi.org/10.1051/0004-6361/202346566

Glassmeier, K., Boehnhardt, H., Koschny, D., Kührt, E., & Richter, I. (2007). The Rosetta Mission : Flying Towards the Origin of the Solar System. *Space Science Reviews*, *128*(1–4), 1–21. https://doi.org/10.1007/s11214-006-9140-8

Goetz, C., Behar, E., Beth, A., Bodewits, D., Bromley, S., Burch, J., Deca, J., Divin, A., Eriksson, A. I., Feldman, P. D., Galand, M., Gunell, H., Henri, P., Heritier, K., Jones, G. H., Mandt, K. E., Nilsson, H., Noonan, J. W., Odelstad, E.,. . . Volwerk, M. (2022). The Plasma Environment of Comet 67P/Churyumov-Gerasimenko. *Space Science Reviews*, *218*(8). https://doi.org/10.1007/s11214-022-00931-1 Jewitt, D. (2022). Destruction of Long-period Comets. *The Astronomical Journal*, *164*(4), 158. https://doi.org/10.3847/1538-3881/ac886d

Hansen, K. C., Altwegg, K., Berthelier, J., Bieler, A., Biver, N., Bockelée-Morvan, D., Calmonte, U., Capaccioni, F., Combi, M. R., De Keyser, J., Fiethe, B., Fougere, N., Fuselier, S. A., Gasc, S., Gombosi, T. I., Huang, Z., Roy, L. L., Lee, S., Nilsson, H.,. . . Wedlund, C. S. (2016). Evolution of water production of 67P/Churyumov-Gerasimenko : An empirical model and a multi-instrument study. *Monthly Notices Of The Royal Astronomical Society*, stw2413. https://doi.org/10.1093/mnras/stw2413

Hartogh, P., Lis, D. C., Bockelée-Morvan, D., De Val-Borro, M., Biver, N., Küppers, M., Emprechtinger, M., Bergin, E. A., Crovisier, J., Rengel, M., Moreno, R., Szutowicz, S., & Blake, G. A. (2011). Ocean-like water in the Jupiter-family comet 103P Hartley 2. *Nature*, *478*(7368), 218–220. https://doi.org/10.1038/nature10519

Henri, P., Vallières, X., Hajra, R., Goetz, C., Richter, I., Glassmeier, K., Galand, M., Rubin, M., Eriksson, A. I., Nemeth, Z., Vigren, E., Beth, A., Burch, J., Carr, C., Nilsson, H.,

Tsurutani, B., & Wattieaux, G. (2017). Diamagnetic region(s) : structure of the unmagnetized plasma around Comet 67P/CG. *Monthly Notices Of The Royal Astronomical Society*, *469*(Suppl_2), S372–S379. https://doi.org/10.1093/mnras stx1540

Jewitt, D., Moro-Martìn, A., & Lacerda, P. (2009). The Kuiper Belt and Other Debris Disks. Dans *Astrophysics and space science proceedings* (p. 53–100). https://doi.org 10.1007/978-1-4020-9457-6_3

Jones, G. H., Snodgrass, C., Tubiana, C., Küppers, M., Kawakita, H., Lara, L. M., Agarwal, J., André, N., Attree, N., Auster, U., Bagnulo, S., Bannister, M., Beth, A., Bowles, N., Coates, A., Colangeli, L., Van Damme, C. C., Da Deppo, V., De Keyser, J.,. . . Del Togno, S. (2024). The Comet Interceptor Mission. *Space Science Reviews*, *220*(1). https://doi.org 10.1007/s11214-023-01035-0

Jewitt, D. (2022b). Destruction of Long-period Comets. *The Astronomical Journal*, *164*(4), 158. https://doi.org/10.3847/1538-3881/ac886d

Koenders, C., Glassmeier, K., Richter, I., Motschmann, U., & Rubin, M. (2013). Revisiting cometary bow shock positions. *Planetary And Space Science*, *87*, 85–95. https:// doi.org/10.1016/j.pss.2013.08.009

Läuter, M., Kramer, T., Rubin, M., & Altwegg, K. (2018). Surface localization of gas sources on comet 67P/Churyumov-Gerasimenko based on DFMS/COPS data. *Monthly Notices Of The Royal Astronomical Society*. https://doi.org/10.1093/mnras/sty3103

Szabó, G. M., Sárneczky, K., & Kiss, L. L. (2011). Frozen to death ? Detection of comet Hale Bopp at 30.7 AU. *Astronomy & Astrophysics*, *531*, A11. https://doi.org 10.1051/0004-6361/201116793

Szabó, G. M., Kiss, L. L., & Sárneczky, K. (2008). Cometary Activity at 25.7 AU : Hale-Bopp 11 Years after Perihelion. *Astrophysical Journal/The Astrophysical Journal*, *677*(2), L121–L124. https://doi.org/10.1086/588095

Vokrouhlický, D., Nesvorný, D., & Dones, L. (2019). Origin and Evolution of Long-period Comets. *The Astronomical Journal*, *157*(5), 181. https://doi.org/10.3847/1538-3881 ab13aa

APPENDIX

Appendix 1: Presentation of the institute

The Swedish Institute of Space Physics IRF (Institutet För Rymdfysik) is a public research institute, linked to the Minister of Education [9] of Sweden.
Its researches are mostly concerning Plasma & Atmospheric Physics, and Space Technologies, which are studied within different sites all over Sweden. The main office is located in Kiruna, the main city in Lapland ; the IRF owns 3 others sites, which are based in Umeå (in the northern Sweden), in Lund (on the west cost), and in Uppsala (on the north of Stockholm).

The IRF is one of the most active research Institute in Sweden, and attracts people from all over the world, this allowing to have a very good international reputation.
Thanks to it, the IRF has been and is implied in various scientific space mission, such as Mars Express, Cluster and Cassini, and more recently in Bepi Colombo, Juice, and Comet Interceptor for instance.

Moreover, the Institute is very implied in the education for the student, from the beginning to the end of the studies. First, they offer courses in space engineering in Kiruna, and in space physics in Uppsala, and give the opportunity to the ones who are passionate aboute space to realize an internship or their master's thesis within their teams. Plus, the students may have the possibility to continue in a four-year Ph.D. after their studies, and even offers postdocs and positions for doctors who want to do research their permanent job.

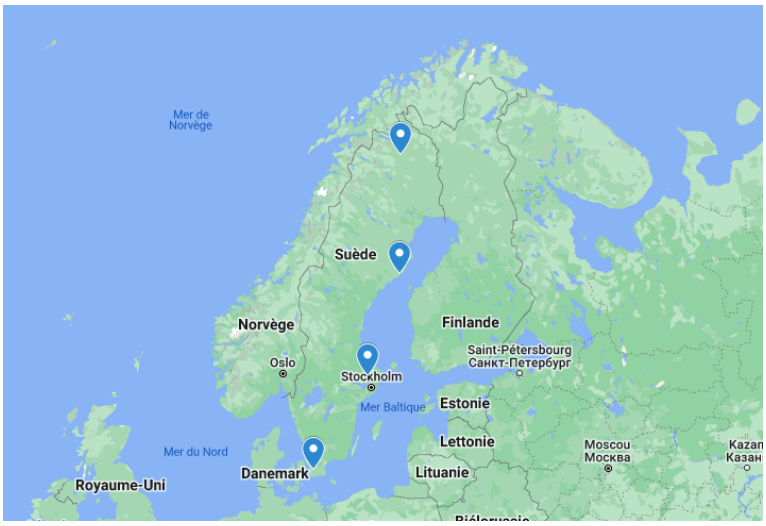

The IRF in Sweden

Sources: IRF – The Swedish Institute of Space physics. (s. d.). https://www.irf.se/en/

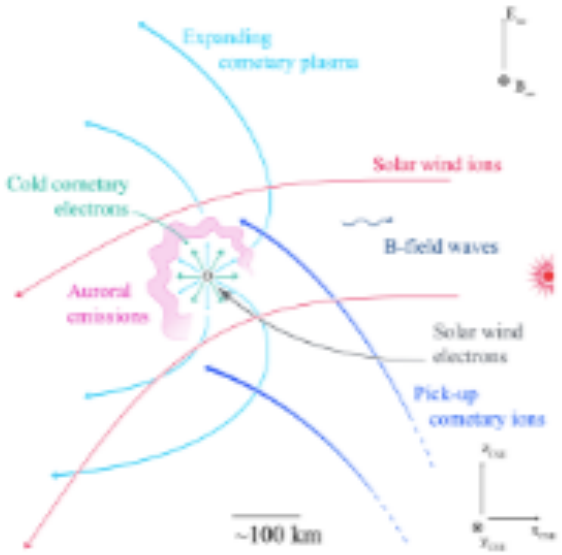

(a) low activity

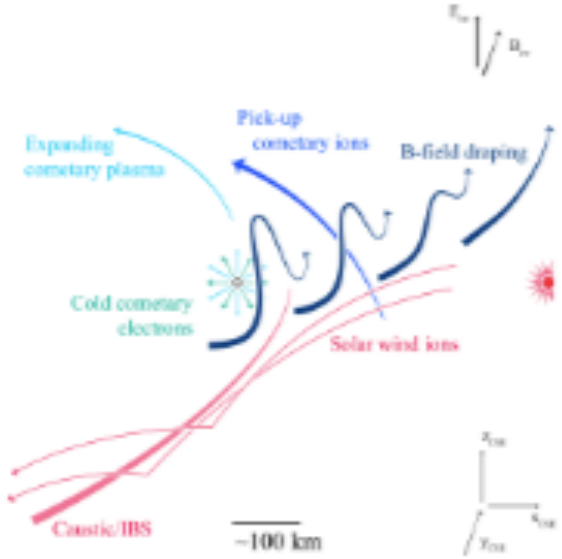

(b) medium activity

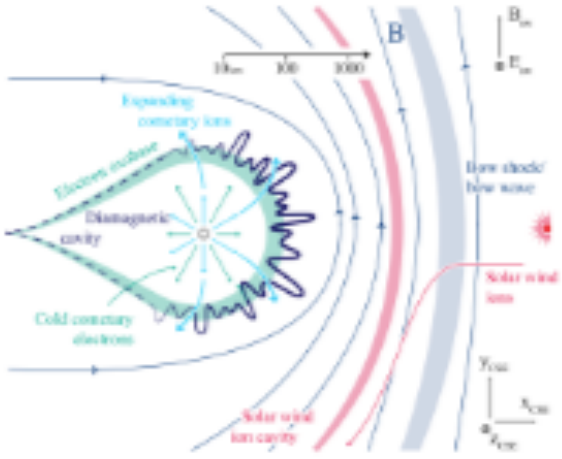

(c) high activity

Appendix 2: Illustration explainning the tree stages of 67P outgassing rate

A summary and overview of the various significant plasma processes can be seen in Appendix 2. The structure around low activity (comet far from the Sun) is illustrated panel a, while the medium and high activity (around the perihelion) ones are illustrated panels b and c respectively. For each of the three activity levels, it displays the key particle trajectories, fields, and phenomena. Both the comet's activity and the plasma conditions vary as they travel through the solar system. For instance, electrons and ions from the solar wind enter the thin atmosphere deeply and can produce auroral emissions at low activity. The asymmetric gyroradius effects of the ions give rise to asymmetric large-scale structures such as the baby bow shock and magnetic field drapeing in the intermediate scenario (panel b). As one gets closer to the Sun (panel c), an unstable diamagnetic cavity forms and cold electrons predominate in the vicinity of the electron exobase. Take note that in this appenix, the majority of waves and electric fields were left off.

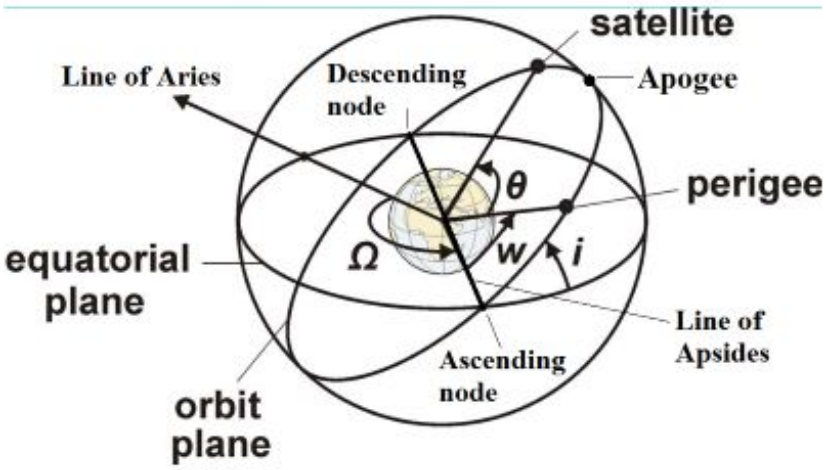

Appendix 3: Illustration showing the main orbital elements in space

On this illustration, the Earth is at the center, but we can easily imagine the same configuration for a comet. We can define 6 parameters to define the trajectory of a celestial body in space (3 positions (x, y, z) in the plan, and 3 angles (i, w, Ω)).
The ascendant node is referring to the point where an orbiting object crosses the plane of reference from south to north ; this plane is considered as the plane of the comet's orbit around the Sun.